# Proposal for automated transformations on single-photon multipath qudits

R. D. Baldijão,[1,2] G. F. Borges,[1] B. Marques,[3] M. A. Solís-Prosser,[4,5] L. Neves,[1] and S. Pádua[1,*]

[1]*Departamento de Física, Universidade Federal de Minas Gerais, Belo Horizonte, MG 31270-901, Minas Gerais, Brazil*

[2]*Instituto de Física Gleb Wataghin, Universidade Estadual de Campinas, Campinas, SP 13083-859, Brazil*

[3]*Instituto de Física, Universidade de São Paulo, SP 05315-970, Brazil*

[4]*Center for Optics and Photonics and MSI-Nucleus on Advanced Optics, Universidad de Concepción, Casilla 4016, Concepción, Chile*

[5]*Departamento de Física, Universidad de Concepción, Casilla 160-C, Concepción, Chile*

(Received 11 July 2017; published 18 September 2017)

We propose a method for implementing automated state transformations on single-photon multipath qudits encoded in a one-dimensional transverse spatial domain. It relies on transferring the encoding from this domain to the orthogonal one by applying a spatial phase modulation with diffraction gratings, merging all the initial propagation paths by using a stable interferometric network, and filtering out the unwanted diffraction orders. The automation feature is attained by utilizing a programmable phase-only spatial light modulator (SLM) where properly designed diffraction gratings displayed on its screen will implement the desired transformations, including, among others, projections, permutations, and random operations. We discuss the losses in the process which is, in general, inherently nonunitary. Some examples of transformations are presented and, considering a realistic scenario, we analyze how they will be affected by the pixelated structure of the SLM screen. The method proposed here enables one to implement much more general transformations on multipath qudits than is possible with a SLM alone operating in the diagonal basis of which-path states. Therefore, it will extend the range of applicability for this encoding in high-dimensional quantum information and computing protocols as well as fundamental studies in quantum theory.

DOI: 10.1103/PhysRevA.96.032329

## I. INTRODUCTION

The physically allowed transformations of quantum states, namely, quantum operations, are one of the basic requirements for any task in quantum information processing and computing [1]. They are also at the core of many fundamental issues in quantum theory, such as the formulation of contextuality in terms of state transformations [2,3].

The optical approaches on these phenomena require the ability to implement operations on the photonic degree of freedom used to encode information. For instance, the single-photon polarization offers the simplicity for dealing with the state transformations, although it is constrained to lie in a two-dimensional Hilbert space. This rules out any possibility of accessing higher-dimensional spaces with single-photon states. That is, with this encoding one is restricted to qubit-based applications only, losing the many advantages that can be exploited from high-dimensional encodings [4–6]. However, the transverse spatial profile of a single-photon multimode field has, in principle, no limit in the information content it can carry out. This can be seen by decomposing the field profile into any infinite orthonormal discrete basis of functions, such as Hermite-Gauss or Laguerre-Gauss functions [7]. In particular, the Laguerre-Gauss decomposition shows that one can encode information in the infinite-dimensional orbital angular momentum (OAM) states of single photons [8]. Restricting this encoding to finite $D$-dimensional subspaces, one generates OAM qudit states which is, currently, one of the main experimental approaches to investigate practical and fundamental issues in quantum mechanics for high-dimensional systems [9–14].

Another successful and, perhaps, simpler approach to encode information in high-dimensional spaces using the photonic spatial degree of freedom is to split its transverse profile into a finite set of $D$ distinguishable spatial modes of propagation. This can be done in many ways, for instance, with a multiport beam splitter [15], an array of slits (or pinholes) [16,17], a multicore optical fiber [18–20], and so on. This type of encoding, which we shall refer to as a *multipath qudit*, may be implemented either in a one-dimensional (1D) spatial domain (e.g., with an array of slits) or in a two-dimensional spatial domain (e.g., with a multicore fiber). Here, we will consider only 1D single-photon multipath qudits.

Recently, the use of programmable spatial light modulators (SLMs) has enhanced the potential for this encoding, providing advances ranging from automated state preparation [21] to automated state transformations [22]. In turn, these advances provided a fertile ground for many recent applications of these multipath qudits such as the demonstration of novel quantum tomographic techniques [23,24], quantum algorithms [25], entanglement characterization [26] and concentration [27], simulation of decoherence [28], quantum key distribution [29], state discrimination [30], and contextuality tests [31–33]. However, regarding the transformations (in which the final state is preserved), so far the operations implemented via SLMs have been restricted to diagonal ones in the basis of which-path states. This brings an unwanted constraint: the impossibility of making a projection while preserving the final state, even though the probability distribution associated with the projection can be obtained with current techniques [24,33]. In addition, they are, in general, state dependent; i.e., if one wants to implement a given transformation on the qudit, the SLM must be configured differently depending on the input state [22,27]. These features, altogether, are limiting and unwanted

*Corresponding author: spadua@fisica.ufmg.br

 

if more general transformations are required. For instance, transformations with nonzero off-diagonal elements could be used to simulate quantum jumps [28]; state-independent operations preserving the final state would be suitable to implement sequential transformations [34,35].

With the goal of extending even more the range of applicability for these 1D single-photon multipath qudits, in this work we propose a method for implementing automated transformations on their states, which will be much more general than the current ones described above. Our method relies on transferring the encoding from the 1D spatial domain, say $x$, to the orthogonal one, $y$. This will be accomplished by applying a spatial phase modulation with diffraction gratings in the $y$ direction, merging all the initial propagation paths in the $x$ direction by using a stable interferometric network, and filtering out the unwanted diffraction orders at the output plane. The automated feature is attained by utilizing a single programmable phase-only SLM, where properly designed diffraction gratings displayed on its screen will implement the desired transformations. We discuss the losses in the process which is, in general, inherently nonunitary, present some examples of transformations, and analyze how they will be affected by the pixelated structure of the SLM screen.

This paper is organized as follows: In Sec. II we briefly review the formalism of quantum operations, define the multipath qudit states encoded in a 1D spatial domain, and present in more detail the limitations regarding previous state transformation on slit states with SLMs. In Sec. III we describe our proposal for automated transformations on these qudits. In Sec. IV we present some examples of possible transformations, discuss how to implement them in practice, and analyze the effects of the pixelation in the SLM. Finally, in Sec. V we conclude and discuss some perspectives.

## II. BASIC CONCEPTS

### A. Quantum operations

Mathematically, operations in quantum states are represented by a linear, completely positive, and trace nonincreasing map $\Lambda$ [1,36] transforming a quantum state $\rho$ into another quantum state $\rho'$, i.e.,

$$\rho \to \rho' = \Lambda(\rho), \tag{1}$$

where $\rho$ and $\rho'$ act on $D$- and $d$-dimensional Hilbert spaces ($\mathcal{H}$ and $\mathcal{H}'$), respectively. The map $\Lambda$ always admits a decomposition called Kraus representation, in which

$$\Lambda(\rho) = \sum_l K_l \rho K_l^\dagger, \tag{2}$$

where $\{K_l\}$ is the set of Kraus operators. For a given $\Lambda$, such a set can always be found with at most $Dd$ elements [36]. They satisfy $\sum_l K_l K_l^\dagger \leqslant \mathbb{I}$, where $\mathbb{I}$ is the identity operator acting on $\mathcal{H}$ and the equality holds for trace-preserving maps.

In the presentation of our proposal in Sec. III, we focus our discussion on transformations ($\mathcal{M}$), both unitary and nonunitary, taking a pure state into another pure state, i.e.,

$$|\psi\rangle \to |\psi'\rangle = \mathcal{M}|\psi\rangle. \tag{3}$$

This expression can be obtained as a special case of (2) where only one Kraus operator acts on the incoming state. In Sec. IV B we shall extend the treatment to more general transformations given by a convex combination of operators, which also shows that this proposal is not limited to pure states.

### B. Single-photon multipath encoded qudits

Let us consider a single-photon multimode field in paraxial and monochromatic approximations propagating along the $z$ direction. Assuming purity, we can write its state in a given transverse plane at $z$ as [7,16,37]

$$|\Psi_z\rangle = \int d\mathbf{x}\, \psi_z(\mathbf{x})|1\mathbf{x}\rangle, \tag{4}$$

where $\mathbf{x} = (x, y)$ is the transverse position coordinate and $\psi_z(\mathbf{x})$ is the field amplitude profile at plane $z$ and satisfies $\int d\mathbf{x}|\psi_z(\mathbf{x})|^2 = 1$. Now, let $\psi_z(\mathbf{x})$ be given by a superposition of Gaussian functions of radius $\omega_z$ centered at $y = 0$ and $x = x_l$ (for $l = 1, \ldots, D$), and complex coefficients $\alpha_l$. Thus, the amplitude is given by

$$\psi_z(\mathbf{x}) = \sum_{l=1}^{D} \alpha_l A \exp\left[-\frac{(x - x_l)^2 + y^2}{\omega_z^2}\right], \tag{5}$$

where $A$ is a normalization factor and $\sum_l |\alpha_l|^2 = 1$. We define the $l$th Gaussian mode displaced in the $x$ direction as

$$\begin{aligned}|\mathcal{X}_l^z\rangle &\equiv \int d\mathbf{x}\, A \exp\left[-\frac{(x - x_l)^2 + y^2}{\omega_z^2}\right]|1\mathbf{x}\rangle \\ &= \int d\mathbf{x}\, G_z(x - x_l) G_z(y)|1\mathbf{x}\rangle,\end{aligned} \tag{6}$$

where $G_z(\xi) = \sqrt{A}\exp(-\xi^2/\omega_z^2)$. Replacing Eqs. (5) and (6) into Eq. (4), we finally arrive at

$$|\Psi_z\rangle = \sum_{l=1}^{D} \alpha_l |\mathcal{X}_l^z\rangle. \tag{7}$$

If $x_l = (l - 1)\chi$ in Eq. (5) and $\chi \gg \sqrt{2}\omega_z$, the overlap between the Gaussians will be negligible and, with good approximation, we will have

$$\langle \mathcal{X}_l^z | \mathcal{X}_j^z \rangle = e^{-\frac{\chi^2(j-l)^2}{2w^2}} \approx \delta_{lj}, \tag{8}$$

so that the states $\{|\mathcal{X}_l^z\rangle\}_{l=1}^D$ will be nearly mutually orthogonal. Therefore, the single-photon state in Eq. (7) will represent a multipath qudit with the information encoded in the paths defined by the Gaussian modes (6) in a 1D spatial domain. This state can be prepared, for instance, by sending a single photon with a collimated Gaussian profile $\psi_z(\mathbf{x})$ through a properly designed set of wave plates and polarizing beam displacers, as recently shown in Refs. [15,34,38–40].

### C. Diagonal operations with a SLM and slit states

Slit states are defined by a discretization of the spatial degree of freedom of photons in a transversal plane. This can be done with single-photon source [29,31–33] as well as twin photons generated by spontaneous parametric down conversion [7,16]. The discretization usually is accomplished

by displaced rectangle functions at the so called image plane. For the single-photon case, the basis states are defined as

$$|l\rangle = \int d\mathbf{x}\,\mathrm{Rect}(x - ld)|1\mathbf{x}\rangle, \tag{9}$$

where $l$ index the basis states, $d$ is the distance between the slits, and $\mathrm{Rect}(x)$ is the rectangle function. Slit states are useful to encode qudits, since the preparation setup is suitable to create high-dimensional states [16,21] and can be automated in both state preparation [21] and transformation [22,24,26,33].

However, manipulation of these states, e.g., slit state transformation, is limited by the fact that an operation transforming any basis state into a linear combination of these states is difficult and has not yet been described. This means that transformations which require $|l\rangle \mapsto \sum_l \alpha_l|l\rangle$, $\sum_l |\alpha_l|^2 \leqslant 1$, are not easy to achieve with this kind of encoding. This implies a limitation to making general transformations, as described in Sec. II A, since they might require that each state component transform into a different linear combination of basis states. Slit state transformations are usually restricted to

$$\mathcal{M}_{\mathrm{Slits}} = \sum_l a_l|l\rangle\langle l|, \tag{10}$$

being represented by diagonal matrices in the slit basis, where $a_l$ are complex coefficients and $\mathcal{M}^\dagger\mathcal{M} \propto \mathbb{I}$. Different experiments have been done with slit states, such as entanglement witness measurement [26], qutrit tomography [24], and contextuality tests [31,33], that measure the statistics of operators not described by Eq. (10). This is done by using the appropriate phase and amplitude manipulation of each state component at the slit basis with a spatial light modulator followed by filtering at the right spot at the Fourier plane. As this is done with programmable SLMs, this process is automated. This method, however, does not deliver the qudit that results from the operation, since the slit encoding is destroyed at the Fourier plane. This kind of limitation forbids sequential operations and quantum dynamics simulation with quantum jumps [28].

This kind of difficulty does not arise, for instance, on Gaussian multipath encoding, described in Sec. II B. State transformations for this kind of encoding are well accomplished by interferometry [15,34], since Gaussian amplitudes are suitable to propagation through larger distances than rectangle amplitudes. However, achieving automation and scalability with hand-made interferometers is a difficult task.

One possibility to enhance the efficiency of these interferometers is the use of photonic chips [41,42], which are integrated and can have adaptable operations [43]. Here we follow a different—while not exclusive—path, where operations are made by a SLM.

## III. TRANSFORMATIONS ON MULTIPATH QUDIT STATES

We now describe our proposal to implement a given operation represented by the matrix $\mathcal{M}$ that transforms the multipath qudit state $|\Psi_z\rangle$ in Eq. (7) in the following way:

$$\mathcal{M} : |\Psi_z\rangle \to |\Psi'_{z'}\rangle = \sum_{l=1}^{d} \beta_l \left|\mathcal{Y}_l^{z'}\right\rangle, \tag{11}$$

where $\sum_l |\beta_l|^2 \leqslant 1$, $d$ is an arbitrary positive integer, and $|\mathcal{Y}_l^{z'}\rangle$ is given by Eq. (6) by replacing $x$ by $y$ and vice versa. The cases where $\sum_l |\beta|^2 < 1$ can be interpreted as a nondeterministic probability of having the intended operation achieved. Equation (11) shows that the initial qudit state, encoded as a superposition of Gaussian modes displaced along the $x$ direction at an input transverse plane $z$, will be transformed into another qudit state given by the superposition of the Gaussian modes along the $y$ direction at an output transverse plane $z'$.

### A. Phase modulation in the $y$ direction

The first key element in our proposal is the use of a phase-only SLM acting on the $y$ direction of the single-photon field profile. Consider a rectangular SLM divided into $D$ non-overlapping rectangular regions of width $a > 2\omega_z$ and centered at $x_l = (l-1)\chi$ for $l = 1, \ldots, D$. At each region we address a given function $\Phi_l(y)$ to be specified later. Thus the transmission function of this SLM can be written as

$$T(\mathbf{x}) = \sum_{l=1}^{D} e^{i\Phi_l(y)}\mathrm{Rect}\left(\frac{x-(l-1)\chi}{a}\right)\mathrm{Rect}\left(\frac{y}{L}\right), \tag{12}$$

where $L$ is the size of the SLM in the $y$ direction and $\mathrm{Rect}(\cdot)$ is the rectangle function. Figure 1 shows an example of a phase mask we shall consider here. The SLM acts according to the polarization state of the incoming field. We assume that the photon is horizontally polarized which will be the working direction of the SLM. With these assumptions, each Gaussian mode $l$ is modulated by the phase function $e^{i\Phi_l(y)}$ only when the photon polarization is horizontal. Photons with vertical polarization are not modulated. Therefore, using Eqs. (5) and (12), the transmitted field profile $\psi_{z_T}(\mathbf{x})$ for the horizontal polarization component will be given by

$$\begin{aligned}\psi_{z_T}(\mathbf{x}) &= T(\mathbf{x})\psi_z(\mathbf{x}) \\ &\approx \sum_{l=1}^{D} \alpha_l G_z(x - x_l)G_z(y)e^{i\Phi_l(y)}.\end{aligned} \tag{13}$$

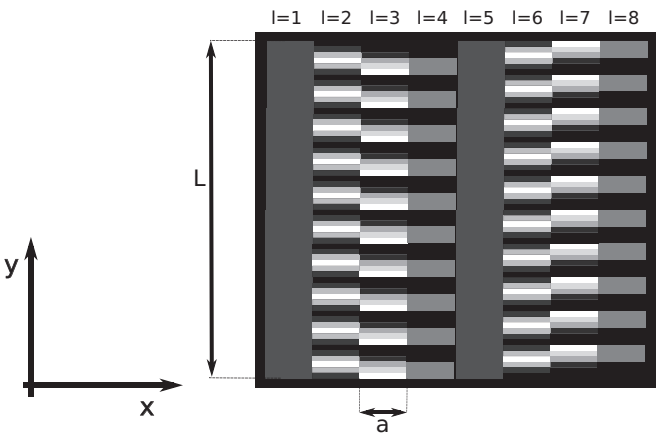


FIG. 1. Example of a phase mask addressed at the SLM that we will consider in this work. Its transmission function is given by Eq. (12) for $D = 8$, where the $\Phi_l(y)$'s are diffraction gratings.

To set the notation for the next discussion, the photon state in a given transverse plane $z_1$ after transmission through the SLM will be

$$\sum_{l=1}^{D} \alpha_l \int d\mathbf{x}\, G_{z_1}(x - x_l)\mathcal{P}_{z_1}\{G_z(y)e^{i\Phi_l(y)}\}|H\rangle|1\mathbf{x}\rangle, \quad (14)$$

where $|H\rangle$ is the horizontal polarization state, that will be explicitly shown in the following calculations; $\mathcal{P}_{z_1}\{\cdot\}$ describes the propagation of the modulated $y$ component of the field profile by a distance $z_1$. Its actual effect will be described later. The $x$ component of the profile, which is not modulated by the SLM, propagates without changing its shape, since we have considered it to be collimated.

### B. Merging the paths in the $x$ direction

The second key element of this proposal is to merge the $D$ paths in the $x$ direction into a single one using the photon polarization as an auxiliary system and the interferometric arrangement similar to the ones in [40,44,45] sketched in Fig. 2. This interferometer is composed by $D-1$ polarizing beam displacers (PBDs), polarizers and optical path compensators, and $2D-2$ half-wave plates (HWPs). In the PBDs we assume that a vertically polarized photon is transmitted without being disturbed while a horizontally polarized one undergoes a lateral displacement in the $x$ direction by a distance $\chi$ equal to the center-to-center separation between neighbor paths. For each PBD, the HWPs before and after it are set to transform the incoming polarization state into $|V\rangle$ and $|H\rangle$, respectively. The optical compensators are birefringent materials that compensate the path length difference between the horizontal and vertical components while the polarizers after the PBDs are used to erase the which-path information, thus ensuring the required interference effect.

Let us see now how the multipath qudit state after the action of the SLM [Eq. (14)] evolves along this setup and how the paths along the $x$ direction are combined by the interferometer. We start the procedure for the paths 1 and 2 in Fig. 2. In path 2, the HWP transforms $|H\rangle \to |V\rangle$. After the PBD and the compensator, paths 1 and 2 are merged and $G_{z_1}(x - x_1) \to G_{z_2}(x - x_2)$. Polarizer 1 projects the photon polarization in this merged path into $\frac{1}{\sqrt{2}}(|H\rangle + |V\rangle)$ and a HWP transforms it back to $|H\rangle$. After all this, the state postselected from the polarization projection becomes

$$\frac{1}{\sqrt{2}}\sum_{l=1}^{2} \alpha_l \int d\mathbf{x}\, G_{z_2}(x - x_2)\mathcal{P}_{z_2}\{G_z(y)e^{i\Phi_l(y)}\}|H\rangle|1\mathbf{x}\rangle + \sum_{l=3}^{D} \alpha_l \int d\mathbf{x}\, G_{z_2}(x - x_l)\mathcal{P}_{z_2}\{G_z(y)e^{i\Phi_l(y)}\}|H\rangle|1\mathbf{x}\rangle, \quad (15)$$

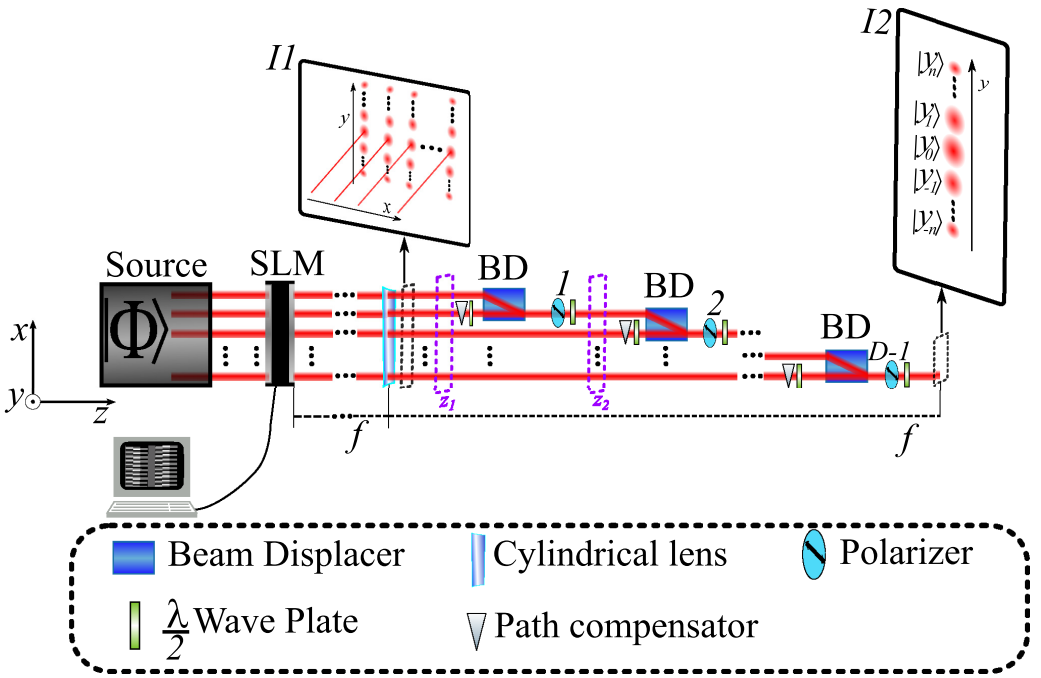


FIG. 2. Sketch of the proposed setup for implementing automated state transformations on single-photon multipath qudit states. A source generates such states encoded in the $x$ direction [see Eq. (7)] with horizontal polarization. A programmable phase-only SLM addressed by a phase mask given by (12) modulates the $y$ component of the field profile, transforming the qudit state into (14). The first inset (I1) shows a representation of the photon path state at this point. The interferometric arrangement described in the text accomplishes the transfer of the encoding from $x$ to $y$ direction, generating the state (17). The cylindrical lens, which has the SLM in its focus, ensures that the diffraction orders will not separate too much and have approximately parallel propagation along the interferometer. It also ensures that they will be described at the posterior focal plane by the Fourier coefficients of the gratings displayed at the SLM screen. The transformations are defined by the phase gratings displayed at the SLM screen, as we show in Sec. III C, and produce the unfiltered state (26). After a proper spatial filtering, the transformation (11) is accomplished, and the transformed multipath qudit state is now encoded in the $y$ direction, as illustrated in the second inset (I2).

where the first term corresponds to the merged paths and the second to the remaining $D-2$ paths. This procedure is iterative: for $p=2,\ldots,D$, the polarization in the path $p$ is transformed as $|H\rangle \to |V\rangle$; then this path is merged with path $p-1$ (which may result from previous mergings) in the $(p-1)$th PBD. In order to erase the path information and minimize losses, the $(p-1)$th polarizer projects the photon polarization into $\frac{1}{\sqrt{p}}(\sqrt{p-1}|H\rangle + |V\rangle)$. Finally, this polarization state is transformed to $|H\rangle$. The general state postselected after these transformations can be written as

$$\frac{1}{\sqrt{p}}\sum_{l=1}^{p}\alpha_l \int d\mathbf{x}\, G_{z_p}(x-x_p)\mathcal{P}_{z_p}\{G_z(y)e^{i\Phi_l(y)}\}|H\rangle|1\mathbf{x}\rangle + \sum_{l=p+1}^{D}\alpha_l \int d\mathbf{x}\, G_{z_p}(x-x_l)\mathcal{P}_{z_p}\{G_z(y)e^{i\Phi_l(y)}\}|H\rangle|1\mathbf{x}\rangle, \tag{16}$$

now, with the first (second) term corresponding to the merged $p$ paths (remaining $D-p$ paths).

Therefore, at the output of the interferometer in Fig. 2, i.e., for $p=D$ in the above description, the postselected state of the output photon will be transformed as

$$|\Psi_z\rangle \to |\Psi'_{z_D}\rangle \equiv \sum_{l=1}^{D}\alpha'_l\left|\mathcal{W}_l^{z_D}\right\rangle, \tag{17}$$

where $\alpha'_l = \alpha_l/\sqrt{D}$ and

$$\left|\mathcal{W}_l^{z_D}\right\rangle = \int d\mathbf{x}\, G_{z_D}(x)\mathcal{P}_{z_D}\{G_z(y)e^{i\Phi_l(y)}\}|1\mathbf{x}\rangle. \tag{18}$$

In Eq. (17) the state $|\Psi'_{z_D}\rangle$ is not normalized, as will be explained in Sec. III C. In the above equation, we dropped the polarization state which will play no role from now on and redefined the origin in the $x$ direction making $x_D = 0$. Note that the spatial mode label $l$ is now only in the $y$ component of the single-photon field profile. Thus, with the whole procedure described so far we were able to transfer the encoding from a one-dimensional transverse spatial domain, $x$, to the orthogonal one, $y$. However, in order to implement the proposed transformation (11), we must be capable of transforming these $D$ modes $|\mathcal{W}_l^{z_D}\rangle$ defined in the $y$ direction into a set of $d$ orthogonal modes, which is our next topic.

As we will see, the $\Phi_l(y)$ functions in the SLM modulating the $y$ component of the field profile will be phase gratings. Thus, for the interferometer to work properly as we described, the generated diffraction orders in the $y$ axis must propagate in parallel to each other and without separating too much (in order to pass through the optical elements). To achieve this, we consider the SLM to be in the focus of a cylindrical lens as shown in Fig. 2.

### C. Creating orthogonal modes in the $y$ direction

In order to discuss the creation of the orthogonal modes in the $y$ direction, we first define the posterior focal plane of the cylindrical lens as our plane of observation after merging the $D$ paths, i.e., $z_D = f$, as shown in Fig. 2. In this case, we replace $\mathcal{P}\{\cdot\} \to \mathcal{F}\{\cdot\}$ in Eq. (18), where $\mathcal{F}\{\cdot\}$ represents the Fourier transform of the field profile in the $y$ direction [46]. At the focal plane we have $k_y = ky/f$, where $k_y$ is the $y$ component of the photon wave vector and $k$ is its wave number. Thus, we can denote the $l$th $y$-component mode function to be computed, as

$$\mathcal{G}_l(y) = \mathcal{F}\{G_z(y')e^{i\Phi_l(y')}\}(k_y). \tag{19}$$

If the $\Phi_l(y')$'s are periodic functions with period $T$, we can expand it into the Fourier series

$$e^{i\Phi_l(y')} = \sum_{j=-\infty}^{\infty} C_{jl}e^{2\pi i j y'/T}, \tag{20}$$

where $C_{jl}$ are the corresponding Fourier coefficients $C_{jl} = \frac{1}{T}\int_0^T dy'\, e^{i\Phi_l(y')}e^{-2\pi i j y'/T}$. Therefore, Eq. (19) becomes

$$\begin{aligned}\mathcal{G}_l(y) &= \sum_{j=-\infty}^{\infty} C_{jl}\mathcal{F}\{G_z(y')e^{2\pi i j y'/T}\}(k_y)\\ &= \sum_{j=-\infty}^{\infty} C_{jl}\mathcal{F}\{G_z(y')\}(k_y - 2\pi j/T)\\ &\equiv \sum_{j=-\infty}^{\infty} C_{jl}\tilde{G}_f\left[\frac{k}{f}(y-y_j)\right],\end{aligned} \tag{21}$$

where $\tilde{G}_f = \mathcal{F}\{G_z\}$ and $y_j = 2\pi j f/Tk$. From Eqs. (17) and (18), the single-photon field profile at the focal plane of the lens, $\psi'_f(\mathbf{x})$, will be given by

$$\begin{aligned}\psi'_f(\mathbf{x}) &= \sum_{l=1}^{D}\alpha'_l\sum_{j=-\infty}^{\infty} C_{jl}G_f(x)\tilde{G}_f\left[\frac{k}{f}(y-y_j)\right]\\ &\equiv \sum_{j=-\infty}^{\infty}\beta'_j G_f(x)\tilde{G}_f\left[\frac{k}{f}(y-y_j)\right],\end{aligned} \tag{22}$$

where, recalling that $\alpha'_l = \alpha_l/\sqrt{D}$,

$$\beta'_j = \frac{1}{\sqrt{D}}\sum_{l=1}^{D}\alpha_l C_{jl}. \tag{23}$$

Since we considered the qudits encoded into Gaussian spatial modes [see Eq. (5)], the Fourier transforms $\tilde{G}_f[(y-y_j)k/f]$ are also Gaussian beams with a waist radius $\omega'_f = 2f/\omega_z k$. The field profile will then be a superposition of Gaussian modes along the $y$ directions separated by a distance $\Delta y = |y_j - y_{j+1}| = 2\pi f/Tk$. If the grating period satisfies $T < \pi\omega_z/2$, the overlap between these Gaussian modes will be negligible and, similarly to Eq. (8),

$$\langle \mathcal{Y}_l^f|\mathcal{Y}_j^f\rangle \approx \delta_{lj}, \tag{24}$$

where

$$\left|\mathcal{Y}_j^f\right\rangle = \int d\mathbf{x}\, G_f(x)\tilde{G}_f\left[\frac{k}{f}(y-y_j)\right]|1\mathbf{x}\rangle. \tag{25}$$

Therefore, using Eqs. (22), (23), and (25), the single-photon state from the interferometer—after the action of the SLM—will be given by

$$|\Psi'_f\rangle = \frac{1}{\sqrt{D}}\sum_{l=1}^{D}\sum_{j=-\infty}^{\infty}\alpha_l C_{jl}\left|\mathcal{Y}_j^f\right\rangle = \sum_{j=-\infty}^{\infty}\beta'_j\left|\mathcal{Y}_j^f\right\rangle. \tag{26}$$

It is important to note that the factor $1/\sqrt{D}$ that arises because of the necessity of erasing the path information generally leads to losses, except in specific cases (such as the projection case, discussed in Sec. IV), and so $0 \leqslant \sum_j |\beta'_j|^2 \leqslant 1$. This implies that there is a probability $p = \sum_j |\beta'_j|^2 \leqslant 1$ of the desired transformation being in fact applied to the incoming state and if further transformations or measurements in the resulting qudit are required, this fact has to be considered.

Comparing Eqs. (11) and (26), one can see that the state transformation $|\Psi_z\rangle \to |\Psi'_f\rangle$ is determined by the Fourier coefficients $\{C_{jl}\}$ obtained from the Fourier expansion of the phase diffraction gratings addressed at the SLM (despite a possible renormalization). More specifically, each coefficient $\beta'_j$ in Eq. (23) of the transformed state is constructed by multiplying each initial state coefficient $\alpha_l$ by the $j$th Fourier coefficient from the $l$th diffraction grating, $C_{jl}$, and adding them together. This means that in order to have a transformation represented by the matrix $\mathcal{M}$ in Eq. (3), it is necessary to choose suitable gratings in order to have $C_{jl} \propto m_{jl}$; each $\Phi_l$ corresponds to the $l$th column of the implemented $\mathcal{M}$. Since the gratings may be generated and controlled in an automated way in the SLM, the transformations proposed here can be completely automated as well.

### D. Spatial filtering

The role of the spatial filtering is to define a finite Hilbert space of dimension $d$ for the resulting transformed state, truncating the sum in expression (26) which takes into account all the diffraction orders. It can be done by filtering out all but $d$ orders, considering the remaining orders as losses. This can be implemented at the output of the interferometer, at the posterior focal plane of the lens (as depicted in the second inset of Fig. 2), or as soon as the orders can be distinguished. For simplicity, we will assume that in either case the same orders are filtered in each path in the $xz$ plane. This is not necessarily the case if one filters the orders before merging the paths with the interferometer. Let us use the following nomenclature: the orders $j$ that are not filtered belong to the interval $j_1 \leqslant j \leqslant j_2$, where $j_2 = j_1 + d - 1$. Then, the fraction of photons that will be lost by spatial filtering is given by

$$\tau_{\mathcal{M}} = \sum_{l=1}^{D} \left( \sum_{m=-\infty}^{j_1-1} |C_{lm}|^2 + \sum_{n=j_2+1}^{\infty} |C_{ln}|^2 \right). \tag{27}$$

It is important to note that this $\tau_{\mathcal{M}}$ factor depends on the operation implemented, represented by the matrix $\mathcal{M}$, and we will see some numeric values for some examples in Sec. IV. The factor $\tau_{\mathcal{M}}$ can also be considered as a reduction of the probability to implement the operation and has to be accounted for, along with $\sum_j |\beta'_j|^2$, if renormalization is required. With the filtering, the state in Eq. (26) is modified as follows:

$$|\Psi_f\rangle = \sum_{l=1}^{D} \sum_{j=j_1}^{j_2} \frac{\alpha_l}{\sqrt{D}} C_{jl} |\mathcal{Y}_j\rangle = \sum_{j'=1}^{d} \beta_{j'} |\mathcal{Y}^f_{j'}\rangle, \tag{28}$$

where $j' = j - j_1 + 1$. We can observe that the elements of the matrix that represents the operation $\mathcal{M}$ are closely related to the coefficients of the Fourier series for each region, i.e., $m_{j'l} \propto C_{jl}$, but now considering only the nonblocked orders. This can be written in matrix form as

$$\begin{bmatrix} m_{11} & m_{12} & \dots & m_{1D} \\ m_{21} & m_{22} & \dots & m_{2D} \\ \vdots & \vdots & \vdots & \vdots \\ m_{d1} & m_{d2} & \dots & m_{dD} \end{bmatrix} = \frac{1}{\sqrt{D}} \begin{bmatrix} C_{j_1 1} & C_{j_1 2} & \dots & C_{j_1 D} \\ C_{(j_1+1)1} & C_{(j_1+1)2} & \dots & C_{(j_1+1)D} \\ \vdots & \vdots & \vdots & \vdots \\ C_{(j_1+d-1)1} & C_{(j_1+d-1)2} & \dots & C_{(j_1+d-1)D} \end{bmatrix}. \tag{29}$$

An operation that has a matrix representation with non-null off-diagonal elements can then be implemented in spatial photonic qudits, and the dimension $d$ of the final state Hilbert space can be different from the Hilbert space of the initial state, in which case $\mathcal{M}$ is not a square matrix. As the transformation is defined by the phase gratings displayed at the SLM screen, the implementation of the operation can be completely automated.

## IV. EXAMPLES AND TECHNIQUES

### A. Some phase gratings and their operation

Equation (29) is the expression that summarizes the main result of this work. It states that the matrix $\mathcal{M}$ representing the transformation applied to the incoming multipath state is completely defined by the phase grating configuration at the SLM. Now we will show explicit examples of matrices $\mathcal{M}$ that can be carried out by a few phase functions, making clear how this proposal is able to implement a large class of automated operations preserving the final state for sequential operations, as discussed in Sec. II C.

Each phase grating $\Phi_l(y)$ at the $l$th path defines the $l$th column of $\mathcal{M}$ by its Fourier coefficients. We will show below some examples of functions with their respective coefficients $\{C_j\}$. These coefficients must be considered as the possible entries of $\mathcal{M}$ ($m_{jl}$) for the specific $\Phi_l$. We will show examples where the Hilbert space dimensions of the initial and final qudit states are equal ($d = D = 3$), and the spatial filtering will select orders $-1 \leqslant j \leqslant 1$. As mentioned in Sec. III though, this is not an intrinsic limitation of the proposal.

#### *1. Sawtooth grating*

The first grating to be considered is the sawtooth phase grating, defined as

$$\Phi(y) = \frac{\varphi y}{T}, \quad 0 \leqslant y \leqslant T, \tag{30}$$

where $\varphi$ is the maximum phase value of the grating and $T$ is the period of the grating. The Fourier coefficients for this idealized continuous grating are given by

$$C_0 = e^{i\varphi/2} \operatorname{sinc}(\varphi/2), \tag{31}$$

$$C_j = e^{i(\varphi/2 - j\pi)} \operatorname{sinc}(\varphi/2 - j\pi). \tag{32}$$

It is important to note that each value of $\varphi$ gives a different set of coefficients, implying a different operation

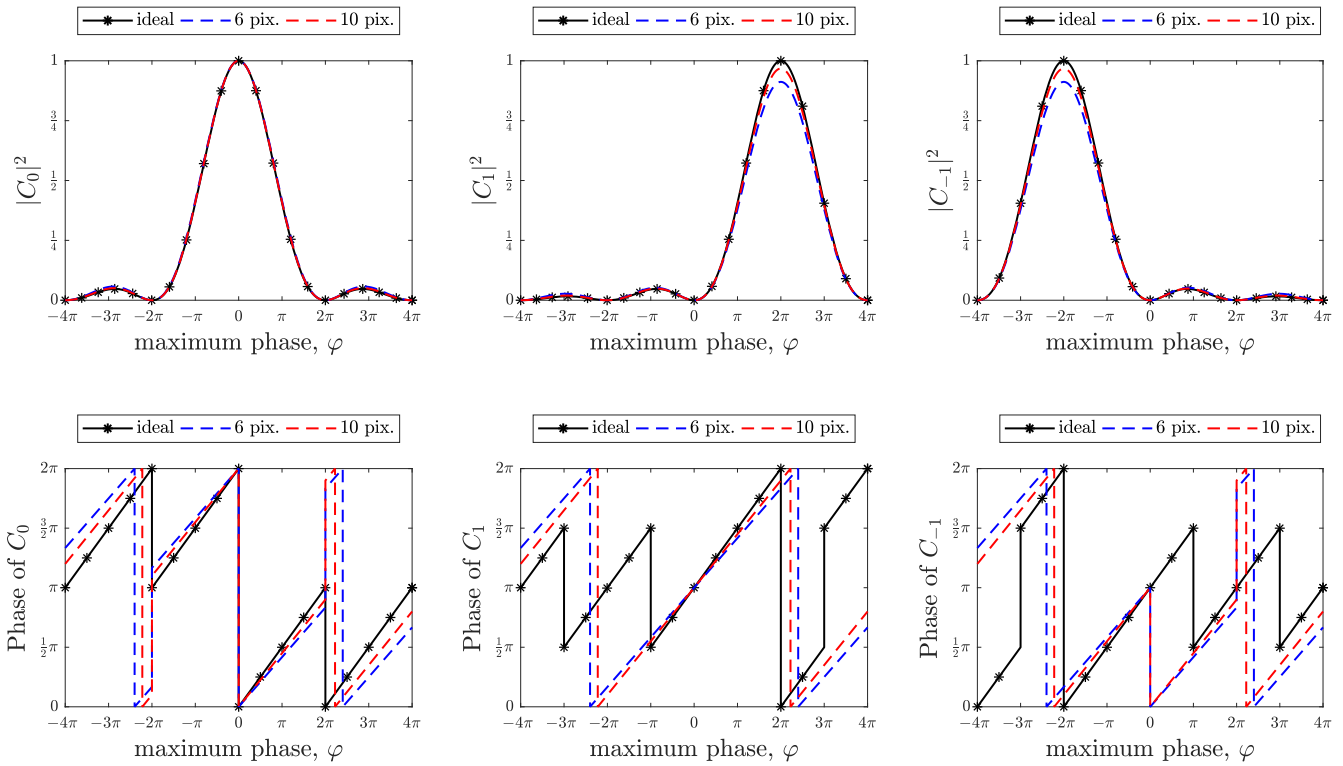


FIG. 3. The coefficients of the linear grating for the ideal (30), $N = 6$, and $N = 10$ pixelated (36) cases as functions of $\varphi$, for the orders $j = 0, \pm 1$. The phase in the plot is modulo $2\pi$. The values of $\varphi$ with negative sign represent the descending sawtooth grating while the positive sign represents an ascending sawtooth grating. For each value of $\varphi$, a different column of the matrix representing the transformation is defined. The interval $\{-4\pi, 4\pi\}$ shows a typical behavior for the orders $j = \pm 1$ and $j = 0$. It is possible to see that this grating can be used at the regions of the SLM in order to make permutation operations, since $C_{\bar{m}} = 1$ for $\varphi = \bar{m}2\pi$, in the ideal case (35). The pixelation affects the diffraction efficiency for the modulus squared and can impinge differences of up to $\pi$ at the phase calculated in the ideal case. In the range and orders used in the examples of this section, the diffraction efficiency is affected by approximately 8% for the $N = 6$ case. In the limit $N \to \infty$ the pixelated and ideal coefficients as functions of $\varphi$ coincide.

implemented in the initial state component ($l$th component). All the coefficients are null for $\varphi = \bar{m}2\pi$ ($\bar{m}$ integer) except for the $C_{\bar{m}}$ coefficient, which is equal to 1. This means that if such a phase grating is used at $l = i$ path, this state component ($|\mathcal{X}_i\rangle\langle\mathcal{X}_i \mid \Psi\rangle$) will be diffracted only to the $\bar{m}$th order, contributing only to the $j = \bar{m}$ component of the final state. For example, if the initial state is

$$|\Psi\rangle = |\mathcal{X}_0\rangle = \begin{pmatrix} 0 \\ 1 \\ 0 \end{pmatrix}_X , \tag{33}$$

and the sawtooth phase grating with $\varphi = 2\pi$ is used only at the non-null initial state component, the final state will be, after renormalization,

$$|\mathcal{Y}_1\rangle = \begin{pmatrix} 1 \\ 0 \\ 0 \end{pmatrix}_Y . \tag{34}$$

This phase grating allows the implementation of permutation operations, such as right and left operations [1]. The $\mathcal{M}$ matrix for the left operation in a 3-dimensional Hilbert space, for example, is

$$\mathcal{M}_{\text{Left}} \propto \begin{pmatrix} 0 & 0 & 1 \\ 1 & 0 & 0 \\ 0 & 1 & 0 \end{pmatrix}, \tag{35}$$

and can be performed by making $\Phi_3(y) = -\Phi_2(y) = 2\pi y/T$ and $\Phi_1(y) = 0$ at the SLM screen. The constant of proportionality is $1/\sqrt{D} = 1/\sqrt{3}$ in this case. The squared modulus, $|C_j|^2$, and the relative phase of each coefficient [phase($C_j$)] to the incoming component are plotted as functions of $\varphi$ in Fig. 3, for $j = 0, \pm 1$, as given by Eq. (32).

These types of transformations (lowering, raising, and permutations) are restrained by the maximum modulation of the SLM. As nowadays SLMs can reach a maximum modulation of approximately $8\pi$, it means that this proposal can be used to get transformations such as (35) up to $d = 8$, with current technology. In cases where only permutations (or computational basis projections as will be explained below) are implemented, the polarizers can be taken out of the setup since there will be no superpositions of different paths, making the expression in (35) an equality, saving losses. However, in this case, the "which-path" information is not erased.

In order to present the examples in a clear way, we considered $\Phi_l$ for the sawtooth grating as being a continuous

function of $y$, for $0 \leqslant y \leqslant T$. However, the SLM screen is pixelated, imposing a discontinuity to the function of the grating, in which each pixel applies a constant phase. In reality, the phase is not applied by the hole pixel, but by a fraction of it, the fill factor. As current SLMs can achieve fill factor $\approx 1$ we will not consider this effect, which generally leads to a small loss in the diffraction efficiency. Calling $N$ the number of pixels in a period, the function for the pixelated sawtooth grating is given by

$$\Phi_n(y') = \sum_{n=0}^{N-1} \varphi \frac{n}{N} \mathrm{Rect}(y' - n - 1/2), \tag{36}$$

where $n$ defines each pixel in a period. This pixeled sawtooth grating function has the following Fourier coefficients:

$$C_0 = \frac{1}{N} e^{i\left(\frac{N-1}{N}\right)\frac{\varphi}{2}} \frac{\sin\left(\frac{\varphi}{2}\right)}{\sin\left(\frac{\varphi}{2N}\right)},$$

$$C_j = \frac{1}{N} \mathrm{sinc}\left(\frac{j\pi}{N}\right) e^{-i\frac{\pi j}{N}} e^{i\frac{N-1}{N}\frac{\varphi - 2\pi j}{2}} \frac{\sin\left(\frac{\varphi}{2} - j\pi\right)}{\sin\left(\frac{\varphi}{2N} - \frac{j\pi}{N}\right)}. \tag{37}$$

The behavior of these coefficients with $\varphi$ for $j = 0, \pm 1$ is given in Fig. 3. The dependency with $N$ has to be carefully analyzed. First, it is important to see that expressions (37) tend to the expressions (32) if $N \to \infty$, as expected. However, this does not mean that the ideal operation is better approximated for higher values of $N$. This happens because the separation between the orders of diffraction is proportional to $\frac{1}{T} = \frac{1}{Nl}$, where $l$ is the size of the pixel in the direction of the periodic behavior of the grating. This means that only increasing the number of pixels is not the best way to have a good experimental result, since the separation between the orders is important in order to obey Eq. (24). It is important to have $N \to \infty$ while $Nl \to T =$ constant, which means smaller pixels. This implies that in order to have a better agreement of the pixeled and idealized functions, it is better to use as high a $T$ as possible in order to ensure the validity of (24). Therefore, SLMs with smaller pixels achieve better results. Second, the presence of the term $\mathrm{sinc}(j\pi/N)$ indicates the decrease in the diffraction efficiency for higher orders ($j \gtrapprox N$). This term also restrains the range of $\varphi$ in which one expects a good agreement between the realistic and ideal scenario. Nonetheless, for the example of the left operation for qutrits shown before, with $N = 12$ one gets $|C_1|^2 = 0.96$ for $\varphi = 2\pi$, given a result of less than 5% of disagreement with the ideal case for the modulus squared.

#### 2. Binary phase grating

Another simple phase grating to use is the binary phase grating represented by the function

$$\Phi(y) = \begin{cases} 0, & 0 \leqslant y < T/2, \\ \varphi, & T/2 \leqslant y < T, \end{cases} \tag{38}$$

with Fourier coefficients given by

$$C_0 = e^{i\frac{\varphi}{2}} \cos(\varphi/2), \tag{39}$$

$$C_j = \begin{cases} \frac{2}{j\pi} e^{i\frac{\varphi}{2}} \sin(\varphi/2), & j \text{ odd}, \\ 0, & m \text{ even}. \end{cases} \tag{40}$$

This phase grating allows the implementation of other transformations. The squared modulus and phases of the coefficients are depicted in Fig. 4.

Using this grating in a qutrit state, with $\varphi = 2\arctan(\pi/2)$ for components $l = 1,2$, and 3 with the addition of a constant phase of value $\pi$ in the $l = 3$ region of the SLM, it is possible to make an operation proportional to the projection in the state $|v\rangle = (1,1,-1)^T$. The proportionality, not an equality, occurs because it is necessary to make use of the filtering described in the previous section. In matrix form,

$$\mathcal{M} \propto \frac{1}{3} \begin{pmatrix} 1 & 1 & -1 \\ 1 & 1 & -1 \\ -1 & -1 & 1 \end{pmatrix}. \tag{41}$$

The constant of proportionality squared $1 - \tau_{\mathcal{M}} = 0.86$ is calculated from (27) and corresponds to the probability of implementing the operation. Other qutrit projections can be obtained with the use of this phase grating and the sawtooth grating. It is important to recall, when considering different operations, that the constant $\tau_{\mathcal{M}}$ depends on the matrix $\mathcal{M}$. The pixelation of the SLM is not considered, since the binary phase grating is itself a discontinuous function of $y$ in a period $T$ and we considered that a half period is constituted of a positive integer number of pixels.

#### 3. Triangular grating

This grating is defined as

$$\Phi(y) = \begin{cases} \frac{-\varphi y}{T}, & -T/2 \leqslant y \leqslant 0, \\ \frac{\varphi y}{T}, & 0 < y \leqslant T/2, \end{cases} \tag{42}$$

with Fourier coefficients given by

$$C_0 = -ie^{i\frac{\varphi}{2}} \mathrm{sinc}(\varphi/2), \tag{43}$$

$$C_j = \frac{-i}{2} e^{i\frac{\varphi + \pi j}{2}} \mathrm{sinc}[(\varphi + \pi j)/2] - \frac{i}{2} e^{i\frac{\varphi - \pi j}{2}} \mathrm{sinc}[(\varphi - \pi j)/2]. \tag{44}$$

The behavior of these coefficients with $\varphi$ is shown in Fig. 5. It is important to note that for this grating $C_{-j} = C_j$, reflecting the symmetry of the function shown in Eq. (42). This grating also has $|C_j|^2$ higher than those of the binary grating for higher orders. With the triangular phase function with $\varphi = 2\pi$ in regions $l = 1,3$ and the spatial filtering of the initial state component $l = 2$ by the proper sawtooth grating it is possible, for example, to make the following operation:

$$\mathcal{M} \propto \frac{1}{2} \begin{pmatrix} 1 & 0 & 1 \\ 0 & 0 & 0 \\ 1 & 0 & 1 \end{pmatrix}, \tag{45}$$

which is proportional to the projection at the $|w\rangle = (1,0,1)^T$ state. In this case, the normalization constant is $\sqrt{1 - \tau_{\mathcal{M}}} = \sqrt{0.36} = 0.6$. It can be seen that the triangular grating is more suitable to make operations with dimensions higher than $d = 3$ for the final state, since $\tau_{\mathcal{M}}$ for orders $|j| \geqslant 2$ is higher for this grating than for the gratings shown before.

We have shown the Fourier coefficients of a triangular grating, allowing for an intuition of what a realistic implementation

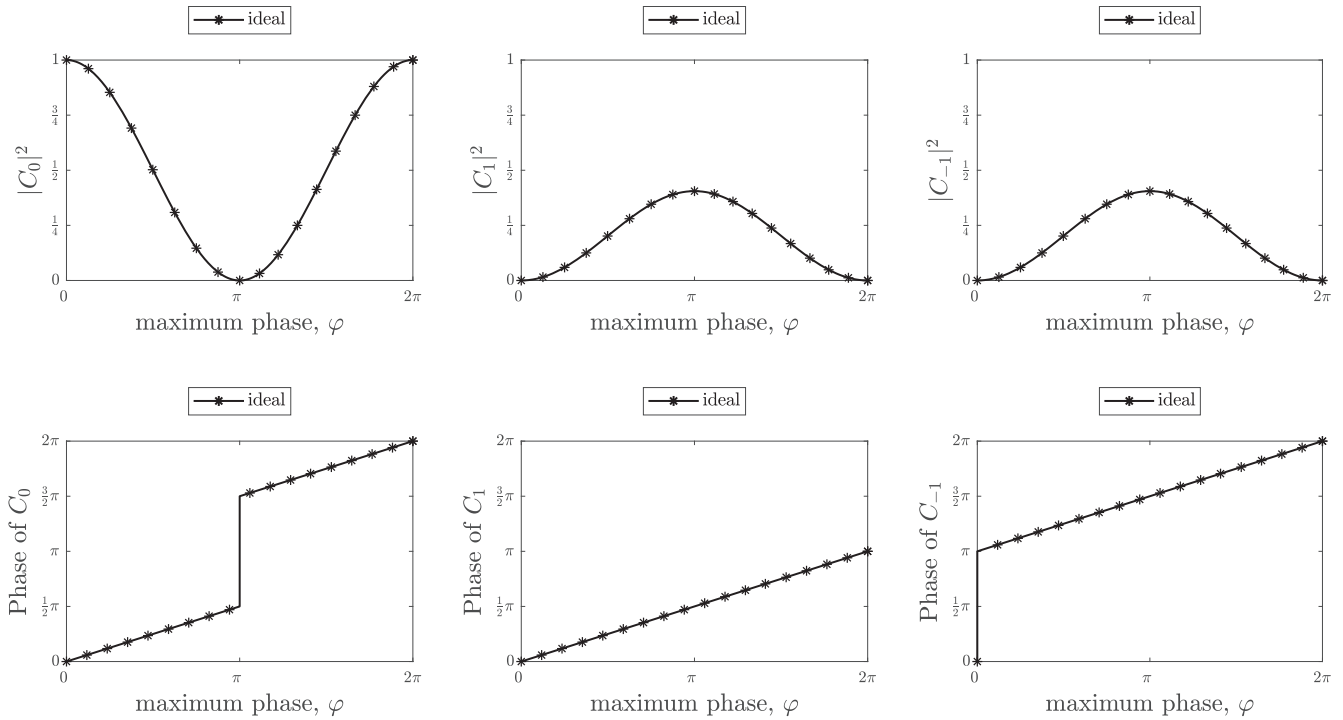


FIG. 4. The behavior of the modulus squared of the coefficients of the binary grating as well as their phase in terms of $\varphi$ for the $j = 0, \pm 1$ orders (40). These grating coefficients are periodic, with period $2\pi$; hence the interval chosen for $\varphi$ in the plots is $\{0, 2\pi\}$. At $\varphi = (2k+1)\pi$, with $k \in \mathbb{N}_+$, the order $j = 0$ is null and changes its phase by $\pi$; all the other orders reach their maximal modulus value. The coefficients of $j < 0$ have the same squared modulus as the $j > 0$ coefficients, but with a phase difference of $\pi$. This grating has $C_j = 0$ for orders with even $j$. We show a qutrit projection possible with this grating for particular values of $\varphi$, using this grating in three regions of the SLM, for a qutrit initial state [Eq. (41)].

would be. Now we will consider the pixelation of the SLM screen. The $\Phi_l$ function is given by

$$\Phi(y') = \begin{cases} \frac{2n\varphi}{N}, & 0 \leqslant n \leqslant \frac{N}{2} - 1; \\ \frac{2n\varphi}{N} - 2\varphi, & \frac{N}{2} \leqslant n \leqslant N - 1, \end{cases} \tag{46}$$

with coefficients given by

$$C_0 = \frac{1}{N} e^{i\frac{\varphi}{2}} \frac{\sin\left(\frac{\varphi}{2}\right)}{\sin\left(\frac{\varphi}{N}\right)} \cos\left(\frac{\varphi}{N}\right), \tag{47}$$

$$C_j = \frac{\operatorname{sinc}\left(\frac{j\pi}{N}\right)}{N} e^{i\frac{\varphi-\pi j}{2}} \left[ e^{-i\frac{\varphi}{N}} \frac{\sin\left(\frac{\varphi-\pi j}{2}\right)}{\sin\left(\frac{\varphi-\pi j}{N}\right)} + e^{i\left(\frac{\varphi}{N}-\pi j\right)} \frac{\sin\left(\frac{\varphi+\pi j}{2}\right)}{\sin\left(\frac{\varphi+\pi j}{N}\right)} \right]. \tag{48}$$

The squared modulus and phase of these coefficients as functions of $\varphi$ are depicted in Fig. 5.

Again, the term $\operatorname{sinc}(j\pi/N)$ restrains the range of orders that leads to results close to the ideal case. But in this more realistic triangular grating, differently from the linear case, the coefficient $C_0$ is equal to 1 for more values of $\varphi$ than in the ideal case. The $\cos(\varphi/N)$ term is responsible for this odd behavior. This term limits the diffraction efficiency and affects the range of orders and values of $\varphi$ in which the pixelated grating approximates to the ideal one. The coefficients (48) for $N \to \infty$ tend to the ideal triangular grating coefficients shown in (44) while when $N = 2$ they become the binary grating coefficients (40), as expected.

These examples show that it is possible to use this proposal to implement different $\mathcal{M}$, transforming the initial state $|\Psi\rangle$ into a different one, $\mathcal{M}|\Psi\rangle$. It becomes a problem of finding the right gratings that have a set of coefficients proportional to the entries of the columns of this matrix. To find these gratings for an arbitrary desired matrix, if possible, is an interesting problem of holography and it is not addressed here. Nonetheless, some intuition can be found by analyzing possible symmetries of the $m_{jl}$ and looking for functions $\Phi(y)$ with coefficients respecting those symmetries in the ideal cases. Then, the realistic pixelated case must be calculated in order to get an accurate result of what will be implemented, considering the number of pixels in a period. For the linear functions we considered we found an analytic form to describe the pixelation effects. However, depending on the mask this can be hard and the coefficients and their deviation to the idealized case may have to be numerically calculated.

In the considerations of the realistic cases, we considered the discretization of the pixelation structure of the screen of the modulator. This is not the only source of discontinuity since the phase scale is also discrete. This discontinuity depends strongly on the function parameters and the gray scale or voltage scale used, and thereby is not considered here. However, depending on the function, configuration, and model of modulator it can be important to account for [47].

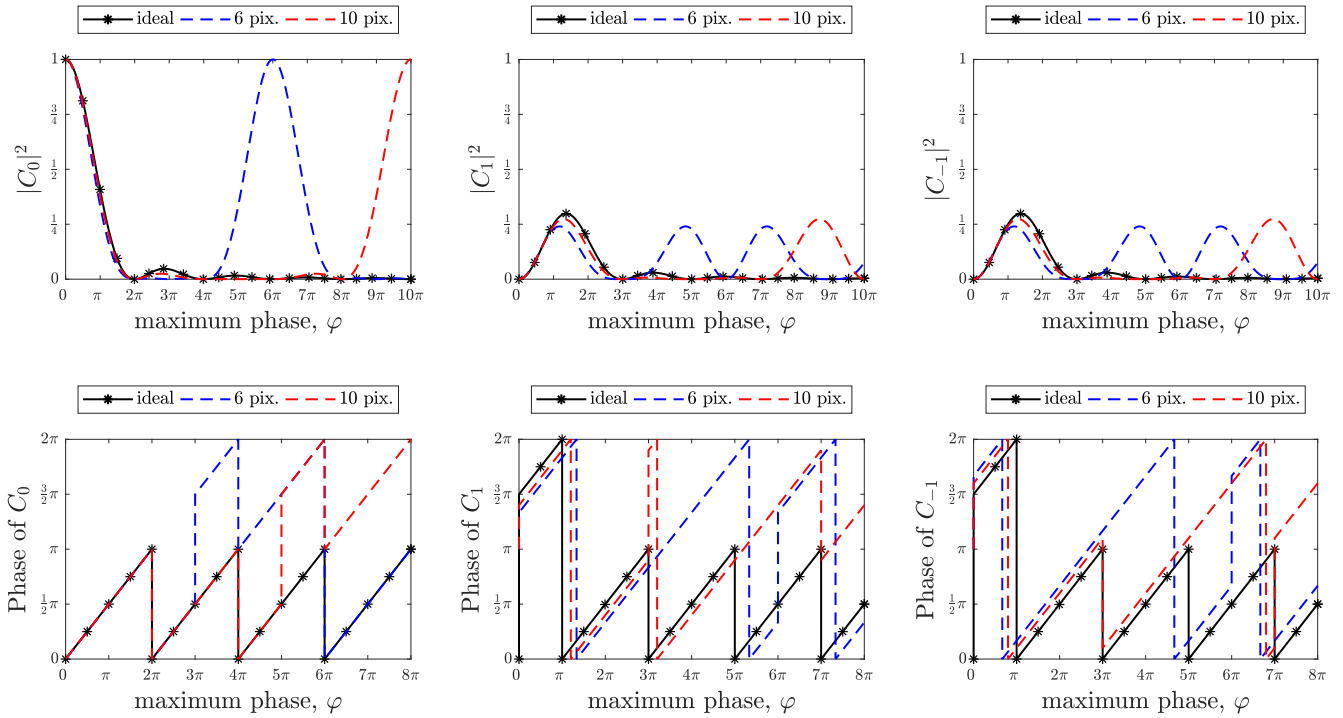


FIG. 5. The behavior of the modulus squared and phases of the coefficients of the ideal and pixelated ($N = 6$ and $N = 10$) triangular gratings as a function of $\varphi$, for the orders $j = 0, \pm 1$ [Eqs. (44) and (48)]. As $\varphi$ goes further from zero, higher orders starts to have $|C_j|^2$ not negligible, making this grating a good candidate to work with higher dimensions for the Hilbert space of the final state. The coefficients of $j < 0$ are identical to the $j > 0$ coefficients and at $\varphi = 2\pi$, the order $j = 0$ for the ideal case is null. However, the differences in the squared modulus due to pixelation can be severe and the plot of the modulus is made up to $\varphi = 10\pi$ to show this effect and its dependence on $\varphi$: $C_0$ reaches unity for more values of $\varphi$ than in the ideal case and $C_j$ is no longer equal to $C_{-j}$, differing by a phase factor. This odd behavior in the modulus happens for higher values of $\varphi$ as $N$ increases and as the phase difference decreases; in the limit $N \to \infty$ the pixelated and ideal coefficients coincide, as expected. The phase plots are made modulo $2\pi$.

Important automated transformations such as permutations and projections for qutrit states were discussed above. Nonetheless, the examples of $\mathcal{M}$ shown do not exhaust the possibilities of operations with these three phase gratings and the same spatial filtering. For example, it is possible to make other qutrit projections, as the projection in the states $(1/\sqrt{2}, 0, -1/\sqrt{2})^T$ or $(-1/\sqrt{3}, 1/\sqrt{3}, 1/\sqrt{3})^T$ with suitable choices of the configuration of the gratings shown in detail in this paper. More transformations can be found, of course, by choosing different phase gratings than the ones given in this section as examples.

### B. Combinations, grating displacement, and more general maps

An important feature of this proposal is that the quantum operations are automated and defined by the diffraction gratings used and thereby unbounded possibilities for transformations can be envisaged. These possibilities, however, are not confined to the different gratings to be used. Combinations of gratings with already calculated coefficients and the use of the same gratings displaced by a distance $a$ can produce new operations [48]. It is also straightforward to produce, with few changes in this setup, a convex sum of operations.

#### *1. Displacing gratings*

Different quantum operations can be realized by displacing a phase grating by an integer number $p$ of pixels or an amount $a = pl$ in the $y$ direction with respect to the known grating, considering $l$ as the size of the pixel in the $y$ direction. Displacement of the phase mask at the SLM screen is already successfully used for preparation of spatial qudits in slightly different ways [48] than the one described in this work. If we write $e^{i\Phi(y')} = f(y')$, and use the superscript $(d)$ for the displaced function, we have

$$C_j^{(d)} = \int_{-\frac{T}{2}}^{\frac{T}{2}} f^d(y') e^{\frac{-2\pi i j}{T} y'} dy'$$

$$= e^{\frac{-2\pi i j}{T} a} \int_{-\frac{T}{2}-a}^{\frac{T}{2}-a} f(y) e^{\frac{-2\pi i j}{T} y} dy = e^{\frac{-2\pi i j}{T} a} C_j. \quad (49)$$

As $a = pl$ and $T = Nl$, we have

$$C_j^{(d)} = e^{\frac{-2\pi i j}{N} p} C_j, \quad (50)$$

where $C_j^{(d)}$ is the coefficient of the displaced grating and $N$ is the total number of pixels in a period $T$. This shows that by displacing transversely the grating (relative to the position of the center of the Gaussian amplitude of the path state component in the $y$ direction) we are able to change the relative phases of the coefficients. This implies that the same grating with the same $\varphi$ can be used to have different $C_j$'s and, thereby, different operations. As an example regarding dimension 2, using the sawtooth grating together with the displacement, it is possible to perform all Pauli matrices with only one SLM.

#### 2. Addition of a transmission SLM in the setup

An interesting possibility that can increase the control of the quantum operations proposed here is to use another transmission phase-only SLM before the interferometer entrance, for example, at the plane $z = z_1$ in Fig. 2. Each diffraction order can be acted on individually if they are already spatially separated at this plane. The second SLM can then change the phase of each coefficient and modify the matrix $\mathcal{M}$. This changes the operation applied from $m_{jl} \propto C_{lj}$ to

$$C_{jl} \mapsto e^{i\Omega_{jl}} C_{jl}, \tag{51}$$

where $\Omega_{jl} \in [0, 2\pi[$ is a phase addressed specifically to each order created by the first SLM. This modification also allows us to correct phase factors that can arise from the propagation of the higher orders through the PBDs.

#### 3. Composition of gratings

Another way of achieving different operations is to combine two gratings to have another one. Suppose the two gratings are described by the functions $\Phi^{(1)}$ and the second $\Phi^{(2)}$. The combined grating will be represented by $\Phi_c = \Phi^{(1)} + \Phi^{(2)}$. This combination does not change the obtained results trivially. However, if one of the combining gratings is a constant phase it is possible to see that the action of this combination is to multiply all the columns of the matrix $\mathcal{M}$ defined by this grating by the constant phase:

$$C_{jl} \overset{\text{composition}}{\longrightarrow} e^{i\theta} C_{jl}. \tag{52}$$

It is important to note that in Eq. (52), the phase modifies equally the entire column of the operation matrix $\mathcal{M}$, which is different from Eq. (51) where the relative phase between each entry of the matrix can be controlled at the expense of an additional modulator.

In the case of a linear grating with $\varphi = 2\bar{m}\pi$ being combined with a grating described by $\Phi^{(1)}(y)$, the effect is to displace the coefficients of $\Phi^1$ by $\bar{m}$. We call $C_j^c$ the coefficient of the composed grating $\Phi_c(y)$. The displacement can be shown as

$$\begin{aligned} C_j^c &= \int_{-\frac{T}{2}}^{\frac{T}{2}} e^{i\Phi_c(y')} e^{\frac{-2\pi i j}{T} y} dy = \int_{-\frac{T}{2}}^{\frac{T}{2}} e^{\frac{2\bar{m}\pi}{T} y} e^{i\Phi^{(1)}(y)} e^{\frac{-2\pi i j}{T} y} dy \\ &= \int_{-\frac{T}{2}}^{\frac{T}{2}} e^{i\Phi^{(1)}(y)} e^{-i\frac{2\pi}{T}(j-\bar{m}) y} dy = C_{(j-\bar{m})}, \end{aligned} \tag{53}$$

where $C_j$ is the coefficient of the $\Phi^{(1)}(y)$ grating.

These two possibilities are useful for achieving the wanted operation without the necessity to look for different phase gratings. However, they are limited by the maximum modulation of the SLM.

#### 4. More general maps

We have considered transformations such as $\rho \to \mathcal{M}\rho\mathcal{M}^\dagger$. Now we address the problem of operations given by maps of the more general form $\rho \to \sum_i K_i \rho K_i^\dagger$. Using the automated characteristic of the SLM this can be made easily if the source of the initial state is not deterministic in time, like in spontaneous parametric down conversion, similarly as described in detail in [28]. In this reference, photonic qudits are prepared in the path variables and the SLM screen is divided in $d$ regions aligned with the paths. A constant phase function is used for each of those regions and different phase masks are changed in time in the SLM screen. If the $i$th mask is displayed by a fraction $t_i$ of the total detection time $T_D$, one can see that the probability $p_i$ of implementing the operation $M_i$, represented by the $i$th phase mask, is proportional to $t_i$. This means that in this case the transformation in the initial state is

$$\rho \to \sum_i p_i \mathcal{M}_i \rho \mathcal{M}_i^\dagger = \sum_i K_i \rho K_i^\dagger, \tag{54}$$

where $K_i = \sqrt{p_i}\mathcal{M}_i$. Comparing (54) with (2) in Sec. II, we see that this proposal can be used to simulate open quantum systems dynamics, if $K_i$ represents correctly the Kraus operators of such dynamics. This was done in Ref. [28] with slit state qudits, and the limitation to diagonal-only transformations made it impossible to simulate maps in which the Kraus decomposition has non-null off-diagonal elements. Applying our proposal to a multipath encoded qudit state this limit is overcome. Then, other open quantum system dynamics simulations can be done if one find the correct phase gratings to implement the Kraus operators of such dynamics.

Another way of having the convex sum of operators acting on the initial state, as in (54), is to use a random number generator with the correct distribution to define the instants in which the operations implemented by the SLM are changed [31–33].

## V. CONCLUSIONS AND PERSPECTIVES

In this work, we present a proposal to have automated operations on multipath photonic qudits encoded in one direction. This is done by using periodic phase gratings on a phase-only SLM and an interferometer that merges the initial path state components into one alone, while the transformed state will be now encoded in the orthogonal direction. Since the operation is controlled and defined only by the phase mask used in the programmable SLM, this proposal is completely automated.

This proposal overcomes the limitation for implementing nondiagonal operations present in the slit states and the dimension limitation present in polarization-encoded qudits. In addition, since there is a wide range of different phase gratings to be used, there are several transformations possible with this proposal. An essential aspect of this proposal is that the final state is preserved for further operations. Therefore, this method can be used to make sequential operations, creating new possibilities for fundamental quantum theory tests, more complex quantum dynamic simulations, and quantum computing protocols.

We also considered the effects of pixelation due to the SLM screen, showing how it affects the results for some phase gratings. This work can be complemented by the use of photonic chips or optical fibers to substitute the interferometer for better control and by a study of the generality of this approach in order to know what operations can be made with this proposal. It would be important to search for an algorithm to find the correct phase function for a given desired matrix operation.

Nonetheless, important operations such as permutations and projections can already be done with this proposal in an automated way using the gratings showed in this paper,

bypassing important difficulties already found in discrete variable quantum optics experiments.

## ACKNOWLEDGMENTS

The authors thank J. Condé for the discussions, comments, and interest in this proposal and M. T. Cunha, R. Rabelo, and A. Cabello for useful discussions and important remarks. This research was supported by CAPES, CNPq, and FAPEMIG. M.A.S.-P. acknowledges financial support from Millennium Scientific Initiative (Grant No. RC130001) and FONDECyT (Grant No. 3170400), and B.M. acknowledges financial support from FAPESP (No. 2014/27223-2). R.D.B. is supported by FAPESP (No. 2016/24162-8).

[1] M. A. Nielsen and I. L. Chuang, *Quantum Information and Quantum Computation* (Cambridge University Press, New York, 2011).

[2] R. W. Spekkens, Contextuality for preparations, transformations, and unsharp measurements, Phys. Rev. A **71**, 052108 (2005).

[3] M. D. Mazurek, M. F. Pusey, R. Kunjwal, K. J. Resch, and R. W. Spekkens, An experimental test of noncontextuality without unphysical idealizations, Nat. Commun. **7**, 11780(E) (2016).

[4] M. Fujiwara, M. Takeoka, J. Mizuno, and M. Sasaki, Exceeding the Classical Capacity Limit in A Quantum Optical Channel, Phys. Rev. Lett. **90**, 167906 (2003).

[5] N. J. Cerf, M. Bourennane, A. Karlsson, and N. Gisin, Security of Quantum Key Distribution Using $d$-Level Systems, Phys. Rev. Lett. **88**, 127902 (2002).

[6] T. Vértesi, S. Pironio, and N. Brunner, Closing the Detection Loophole in Bell Experiments Using Qudits, Phys. Rev. Lett. **104**, 060401 (2010).

[7] S. P. Walborn, C. H. Monken, S. Pádua, and P. H. Souto Ribeiro, Spatial correlations in parametric down-conversion, Phys. Rep. **495**, 87 (2010).

[8] M. Krenn, M. Malik, T. Scheidl, R. Ursin, and A. Zeilinger, *Quantum Communication with Photons* (Springer International Publishing, Cham, 2016), pp. 455–482.

[9] M. Mirhosseini, M. Malik, Z. Shi, and R. W. Boyd, Efficient separation of the orbital angular momentum eigenstates of light, Nat. Commun. **4**, 2781 (2013).

[10] G. C. G. Berkhout, M. P. J. Lavery, J. Courtial, M. W. Beijersbergen, and M. J. Padgett, Efficient Sorting of Orbital Angular Momentum States of Light, Phys. Rev. Lett. **105**, 153601 (2010).

[11] N. González, G. Molina-Terriza, and J. P. Torres, How a Dove prism transforms the orbital angular momentum of a light beam, Opt. Express **14**, 9093 (2006).

[12] A. Vaziri, G. Weihs, and A. Zeilinger, Superpositions of the orbital angular momentum for applications in quantum experiments, J. Opt. B: Quantum Semiclassical Opt. **4**, S47 (2002).

[13] A. Babazadeh, M. Erhard, F. Wang, M. Malik, R. Nouroozi, M. Krenn, and A. Zeilinger, High-dimensional single-photon quantum gates: Concepts and experiments, arXiv:1702.07299.

[14] M. Agnew, E. Bolduc, K. J. Resch, S. Franke-Arnold, and J. Leach, Discriminating Single-Photon States Unambiguously in High Dimensions, Phys. Rev. Lett. **113**, 020501 (2014).

[15] M. Reck, A. Zeilinger, H. J. Bernstein, and P. Bertani, Experimental Realization of Any Discrete Unitary Operator, Phys. Rev. Lett. **73**, 58 (1994).

[16] L. Neves, G. Lima, J. G. Aguirre Gómez, C. H. Monken, C. Saavedra, and S. Pádua, Generation of Entangled States of Qudits Using Twin Photons, Phys. Rev. Lett. **94**, 100501 (2005).

[17] S. P. Walborn, D. S. Lemelle, M. P. Almeida, and P. H. Souto Ribeiro, Quantum Key Distribution with Higher-Order Alphabets Using Spatially Encoded Qudits, Phys. Rev. Lett. **96**, 090501 (2006).

[18] M. N. O'Sullivan-Hale, I. A. Khan, R. W. Boyd, and J. C. Howell, Pixel Entanglement: Experimental Realization of Optically Entangled $d = 3$ and $d = 6$ Qudits, Phys. Rev. Lett. **94**, 220501 (2005).

[19] Y. Ding, D. Bacco, K. Dalgaard, X. Cai, X. Zhou, K. Rottwitt, and L. K. Oxenløwe, High-dimensional quantum key distribution based on multicore fiber using silicon photonic integrated circuits, npj Quantum Information **3**, 25 (2017).

[20] G. Cañas, N. Vera, J. Cariñe, P. González, J. Cardenas, P. W. R. Connolly, A. Przysiezna, E. S. Gómez, M. Figueroa, G. Vallone, P. Villoresi, T. Ferreira da Silva, G. B. Xavier, and G. Lima, High-dimensional decoy-state quantum key distribution over multicore telecommunication fibers, Phys. Rev. A **96**, 022317 (2017).

[21] M. A. Solís-Prosser, A. Arias, J. J. M. Varga, L. Rebòn, S. Ledesma, C. Iemmi, and L. Neves, Preparing arbitrary pure states of spatial qudits with a single-phase-only spatial light modulator, Opt. Lett. **38**, 4762 (2013).

[22] G. Lima, A. Vargas, L. Neves, R. Guzmán, and C. Saavedra, Manipulating spatial qudit states with programmable optical devices, Opt. Express **17**, 10688 (2009).

[23] G. Lima, L. Neves, R. Guzmán, E. S. Gómez, W. A. T. Nogueira, A. Delgado, A. Vargas, and C. Saavedra, Experimental quantum tomography of photonic qudits via mutually unbiased basis, Opt. Express **19**, 3542 (2011).

[24] W. M. Pimenta, B. Marques, M. A. D. Carvalho, M. R. Barros, J. G. Fonseca, J. Ferraz, M. Terra Cunha, and S. Pádua, Minimal state tomography of spatial qubits using a spatial light modulator, Opt. Express **18**, 24423 (2010).

[25] B. Marques, M. R. Barros, W. M. Pimenta, M. A. D. Carvalho, J. Ferraz, R. C. Drumond, M. Terra Cunha, and S. Pádua, Double-slit implementation of the minimal Deutsch algorithm, Phys. Rev. A **86**, 032306 (2012).

[26] A. J. Gutiérrez-Esparza, W. M. Pimenta, B. Marques, A. A. Matoso, J. Sperling, W. Vogel, and S. Pádua, Detection of nonlocal superpositions, Phys. Rev. A **90**, 032328 (2014).

[27] B. Marques, A. A. Matoso, W. M. Pimenta, A. J. Gutiérrez-Esparza, G. Lima, L. Neves, A. Delgado, C. Saavedra, and S. Pádua, Optimal entanglement concentration for photonic qutrits encoded in path variables, Phys. Rev. A **87**, 052327 (2013).

[28] B. Marques, A. A. Matoso, W. M. Pimenta, A. J. Gutiérrez-Esparza, M. F. Santos, and S. Pádua, Experimental simulation of decoherence in photonics qudits, Sci. Rep. **5**, 16049(E) (2015).

[29] S. Etcheverry, G. Cañas, E. S. Gómez, W. A. T. Nogueira, C. Saavedra, G. B. Xavier, and G. Lima, Quantum key distribution

session with 16-dimensional photonic states, Sci. Rep. **3**, 2316 (2013).

[30] M. A. Solís-Prosser, M. F. Fernandes, O. Jiménez, A. Delgado, and L. Neves, Experimental Minimum-Error Quantum-State Discrimination in High Dimensions, Phys. Rev. Lett. **118**, 100501 (2017).

[31] G. Cañas, E. Acuña, J. Cariñe, J. F. Barra, E. S. Gómez, G. B. Xavier, G. Lima, and A. Cabello, Experimental demonstration of the connection between quantum contextuality and graph theory, Phys. Rev. A **94**, 012337 (2016).

[32] M. Arias, G. Cañas, E. S. Gómez, J. F. Barra, G. B. Xavier, G. Lima, V. D'Ambrosio, F. Baccari, F. Sciarrino, and A. Cabello, Testing noncontextuality inequalities that are building blocks of quantum correlations, Phys. Rev. A **92**, 032126 (2015).

[33] G. Cañas, M. Arias, S. Etcheverry, E. S. Gómez, A. Cabello, G. B. Xavier, and G. Lima, Applying the Simplest Kochen-Specker Set for Quantum Information Processing, Phys. Rev. Lett. **113**, 090404 (2014).

[34] A. Cabello, E. Amselem, K. Blanchfield, M. Bourennane, and I. Bengtsson, Proposed experiments of qutrit state-independent contextuality and two-qutrit contextuality-based nonlocality, Phys. Rev. A **85**, 032108 (2012).

[35] B. Marques, J. Ahrens, M. Nawareg, A. Cabello, and M. Bourennane, Experimental Observation of Hardy-Like Quantum Contextuality, Phys. Rev. Lett. **113**, 250403 (2014).

[36] K. Kraus, *States, Effects, and Operations: Fundamental Notions of Quantum Theory* (Springer, Berlin, 1983).

[37] C. H. Monken, P. H. Souto Ribeiro, and S. Pádua, Transfer of angular spectrum and image formation in spontaneous parametric down-conversion, Phys. Rev. A **57**, 3123 (1998).

[38] E. Amselem, Dynamics of quantum correlations with photons, Ph.D. thesis, University of Stockholm, 2011.

[39] X. Zhan, X. Zhang, J. Li, Y. Zhang, B. C. Sanders, and P. Xue, Realization of the Contextuality-Nonlocality Tradeoff with a Qubit-Qutrit Photon Pair, Phys. Rev. Lett. **116**, 090401 (2016).

[40] X. M. Hu, J. S. Chen, B. H. Liu, Y. Guo, Y. F. Huang, Z. Q. Zhou, Y. J. Han, C. F. Li, and G. C. Guo, Experimental Test of Compatibility-Loophole-Free Contextuality with Spatially Separated Entangled Qutrits, Phys. Rev. Lett. **117**, 170403 (2016).

[41] L. Sansoni, F. Sciarrino, G. Vallone, P. Mataloni, A. Crespi, R. Ramponi, and R. Osellame, Polarization Entangled State Measurement on a Chip, Phys. Rev. Lett. **105**, 200503 (2010).

[42] A. Politi, M. J. Cryan, J. G. Rarity, S. Yu, and J. L. O'Brien, Silica-on-silicon waveguide quantum circuits, Science **320**, 646 (2008).

[43] F. Flamini, L. Magrini, A. S. Rab, N. Spagnolo, V. D'Ambrosio, P. Mataloni, F. Sciarrino, T. Zandrini, A. Crespi, R. Ramponi, and R. Osellame, Thermally reconfigurable quantum photonic circuits at telecom wavelength by femtosecond laser micromachining, Light Sci. Appl. **4**, e354 (2015).

[44] J. L. O'Brien, G. J. Pryde, A. G. White, T. C. Ralph, and D. Branning, Demonstration of an all-optical quantum controlled-not gate, Nature (London) **426**, 264 (2003).

[45] M. A. Broome, A. Fedrizzi, B. P. Lanyon, I. Kassal, A. Aspuru-Guzik, and A. G. White, Discrete Single-Photon Quantum Walks with Tunable Decoherence, Phys. Rev. Lett. **104**, 153602 (2010).

[46] J. W. Goodman, *Introduction to Fourier Optics*, 2nd ed. (McGraw-Hill Companies, New York, 1996).

[47] I. Moreno, C. Iemmi, A. Márquez, J. Campos, and M. J. Yzuel, Modulation light efficiency of diffractive lenses displayed in a restricted phase-mostly modulation display, Appl. Opt. **43**, 6278 (2004).

[48] J. J. M. Varga, L. Rebón, M. A. Solís-Prosser, L. Neves, S. Ledesma, and C. Iemmi, Optimized generation of spatial qudits by using a pure phase spatial light modulator, J. Phys. B **47**, 225504 (2014).